Available online at www.CivileJournal.org

Civil Engineering Journal

(E-ISSN: 2476-3055; ISSN: 2676-6957)

Vol. 9, No. 12, December, 2023

Effect of Silane and Silicate based Penetrants against Corrosion of Steel with Partial Cover Thickness

Muhammad Afaq Khalid [1*], Shinichi Miyazato [1], Tatsuya Minato [1], Hibiki Mizuguchi [1]

[1] *Department of Environmental and Civil Engineering, Kanazawa Institute of Technology, Nonoichi 921-8501, Japan.*

Received 20 August 2023; Revised 22 November 2023; Accepted 27 November 2023; Published 01 December 2023

Abstract

The partial cover thickness of reinforced concrete structures near the coastline enhances the early corrosion onset, which reduces the service life. As a countermeasure under the preventive maintenance approach, to delay early corrosion onset in structures with partial cover thickness and increase durability throughout the service life, this study used silane and silicate-based surface penetrants. Mortar specimens with a partial cover thickness and embedded, specially segmented bars were prepared. Both penetrants were applied to specimens with partial cover thicknesses (20 and 7.5 mm). Further, electrochemical methods such as macrocell current, microcell current, electric resistivity, and potentiodynamic polarization curves were used to assess the corrosion resistance before and after coating. The penetration depth of silane was measured visually, and the Vickers hardness test was used for the silicate penetrant. The "equivalent cover approach" was adopted to evaluate the performance of penetrants throughout their service lives. Results revealed that the total corrosion current density decreased by 79% for specimens coated with silane and 52% for silicate penetrant, whereas no change was observed in the uncoated specimens. Based on the equivalent cover approach, the silane penetrant was determined to be most effective in delaying the corrosion onset and propagation time for cover thicknesses of 60 and 50 mm at 100 m distance against 70 mm, and for 40 and 30 mm against 50 mm at 250 m from the coastline. Further, the silicate-based penetrant was only effective for a deficient cover thickness of 5 mm against the specified cover thicknesses at a distance of 100 and 250 m from the sea coast.

Keywords: Cementitious Material; Corrosion Rate; Corrosion Onset; Silane Surface Penetrant; Silicate Surface Penetrant.

1. Introduction

The concrete cover in Reinforced Concrete (RC) structures protects steel from external environmental effects, preserves passive film, and maintains the bar in a highly alkaline state. At the construction stage, if the specified cover thickness, including the allowable tolerances [1–3], is not achieved, a variable/partial cover thickness is constructed at different sections of the structural member. Owing to the porous matrix and variable thickness of the concrete cover, the chloride ions and moisture in marine and de-icing salts should penetrate non-uniformly. This non-uniform penetration of chloride ions at different cover thicknesses reaches the steel surface by destroying the passive film and initiating corrosion when the chloride ion concentration exceeds the threshold. This partial cover thickness induces early corrosion onset [4], and timely intervention is required to delay corrosion onset and maintain the structure throughout its service life.

The durability of RC structures depends on the characteristics of the cover [5] and primarily on the thickness and strength of the materials used. Steel embedded in a less impervious and thicker cover requires a long time to corrode and, hence, a longer service life of the RC structure [6]. A thin passive film of iron oxide in a highly alkaline environment

* Corresponding author: c7000029@planet.kanazawa-it.ac.jp

http://dx.doi.org/10.28991/CEJ-2023-09-12-02

protects the rebar against corrosion [7], which can be damaged by aggressive agents such as water and chloride ions. Water and chloride ingress could be the main causes of the corrosion initiation of steel in concrete [8–9]. The main sources of chloride ions are deicing agents and chloride ions, which may also be transported via vehicles that travel from snow-bound areas to urban areas and transport deicing agents through tires. The well-known Tutti 1982 graphical presentation describing the service life of RC structures can be categorized into two stages: corrosion onset or initiation and the period of corrosion propagation [10]. The corrosion initiation period describes the transport of corrosive agents, such as chloride ions, through the concrete at the depth of the rebar and when it reaches a threshold value of 1.9 kg/m^3 as per standard specifications and guidelines for the durability design of concrete structures in Japan [11] for a water-cement ratio (W/C) of 0.50. As corrosion propagates after initiation, the propagation period is defined as the time between initiation and steel destruction and is dependent on the corrosion onset. The propagation period is relatively short compared to the first stage [12–13]. The corrosion initiation period for a structure with a low W/C ratio (0.30) has been reduced by 65 years for a short cover depth of 30 mm compared with a 50 mm cover depth at a distance of 500 m from the coastline [14].

Structures are usually limited in their service life until the end of the initiation phase; that is, when the passive steel layer is broken, corrosion begins. There are two types of corrosion of the steel reinforcement in concrete-based on the spatial arrangement of the electrochemical cells: macrocell and microcell corrosion. Macrocell corrosion occurs for two primary reasons: when the passive film that protects the steel bar is damaged, and owing to the chloride ion concentration difference during the diffusion process [15]. If a part of a single bar extends outside the concrete, it can result in macrocell corrosion [16]. During microcell corrosion, the cathodic and anodic areas coexist in close proximity. The sum of the anodic macrocell and microcell for a single steel element is called the total corrosion current density [17, 18].

Therefore, the most important period under consideration is from construction to corrosion initiation, and timely intervention can increase the service life and durability of RC structures. A solution to this problem could be to prevent the penetration of chloride ions and water into the concrete, resulting in delayed corrosion initiation. Based on this concept, several concrete surface treatments have been developed [19–21]. Silane-based penetrants are widely used owing to their high durability, water resistance, and aesthetics of the finished surface [22, 23]. When a silane penetrant is applied to the concrete surface, it forms an impervious layer that prevents the transportation of water and chloride ion solutions [24–26]. In Niigata Prefecture, Japan, the sound barriers of the Shinkansen structure were coated with silane penetrants, which were exposed to cold winters and hot summers. Following 8 years of conducting exposure tests, the silane penetrants performed exceptionally well against waterproofing [27]. Zhao et al. (2022) reported that a substrate treated with silane impregnation exhibited a protective effect for up to 20 years [28]. Silane-based surface penetrants possess high resistance to chloride ion penetration [29]. Surface penetrants based on silanes were more effective at preventing chloride ion diffusion than acrylic coatings [30]. Many researchers have reported the influence of silane-based surface penetrants on steel corrosion. More than half of the corrosion current was reduced by a silane-based surface penetrant [31–33]. According to Sivasankar et al. (2013) [34], the silane surface penetrant extended the corrosion time of reinforcement by approximately four times, and this effect was influenced by the molecular size of the hydrophobic agent. Furthermore, chloride ion diffusion in the substrate can be decreased by treatment with silane penetrants; this effect increases with increasing concentrations of the active product [35].

Surface penetrants of the silicate-based material have been used for many years in buildings and on highway bridges [36]. Sodium silicate is among the most commonly used pore-blocking surface treatments. Studies [37–39] have concluded that sodium silicate improves the durability of concrete. However, certain studies [36, 40] reported that silicate-based surface penetrants cannot significantly prevent the diffusion of chloride ions and water owing to the occurrence of microcracks on the surface of the concrete. The silicate-based surface penetrant reacts with calcium hydroxide in concrete to form insoluble colloidal silica gel (C-S-H), which blocks the pores of the concrete substrate, thus increasing its durability and impermeability of the concrete substrate. According to Franzoni et al. (2013) [41], treatment with sodium silicate decreases the depth of chloride migration by 30–50%. During an exposure period of 20 years to ultraviolet light and other environmental conditions, the performance of mortar specimens coated with silicate penetrant was investigated. It was found that chloride ion penetration increased in the mortar specimens after the 10th year, and water permeability increased after the 20th year. The authors recommended recoating after 10 years in a chloride environment [42]. The life cycle of concrete coated with silicate-based surface penetrant is approximately twice as long, and the coefficient of diffusion of chloride ions is nearly 50% lower than that of an uncoated concrete surface [43]. Based on the results of these studies, the performance of silane and silicate-based penetrants against reinforcement corrosion owing to chloride ion diffusion and water permeability has been identified. However, the effect of penetrants on the corrosion of bars with partial cover thickness in a chloride environment remains unknown.

Therefore, this study quantitatively measured the effect of silane and silicate-based surface penetrants on the corrosion of a special segmented bar with partial cover thickness simulated as initial defects during the construction stage by employing electrochemical methods such as macrocell current, polarization resistance, electric resistivity, and polarization curves. To simulate the partial cover thickness defect in actual structures, the specimen was cast in a cylindrical shape at two different depths (20, 7.5 mm), and a specially segmented bar, which was electrically connected,

was embedded. The penetration depth of the silane was measured visually, and the Vickers hardness index was used to determine the penetration depth of the silicate-based penetrant. Finally, using the experimental data, an equivalent cover approach based on Fick's 2nd law of diffusion was used to calculate the corrosion onset and propagation times for RC structures 100 and 250 m from the coastline. Consequently, recommendations were made based on experimental data and case studies to help engineers choose an appropriate type of surface penetrant for a particular cover based on the cost-benefit ratio.

2. Experimental Program

The experimental setup is shown in Figure 1. This chart presents the experimental flow and simulation results. Electrochemical tests were conducted before and after the specimens were coated. The corrosion rates, penetration depths from the experiments, and diffusion coefficients of the penetrants and substrate were substituted in the equation to use the equivalent cover approach (JSCE guidelines), and the corresponding equivalent cover depths were calculated and analyzed at 100 and 250 m from the coastline.

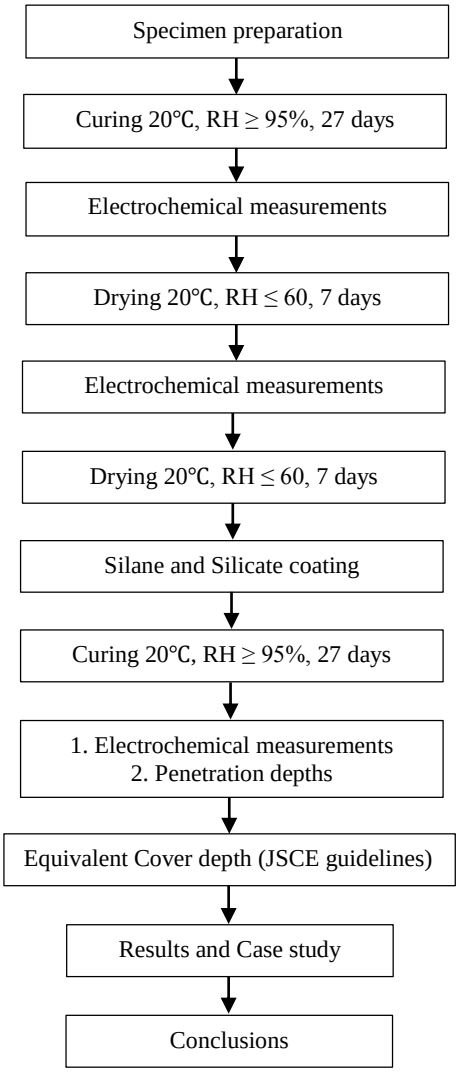

Figure 1. Flow chart showing the research flow and methodology

2.1. Materials

2.1.1. Specimen Details

To measure the localized corrosion current, a specimen was prepared using a specially divided deformed bar (SD 295 in JIS G 3112) with a nominal diameter of 10 mm. Six 25-mm steel elements were soldered with lead wires of different colors at both ends of each steel element. The soldered ends were coated with a high-epoxy resin-insulating material to prevent local corrosion. Individual steel elements were fabricated using epoxy to form a 180-mm-long bar, as shown in Figure 2(a), serving as a single electrically connected bar. The resistivity of each steel element was measured to be less than 0.5 Ω, as proposed by Miyazato & Otsuki (2010) [44]. A polyvinyl chloride (PVC) pipe was used as the mold, as shown in Figure 2(b). Further, a 180-mm-long special divided bar was fixed at the center using bamboo sticks and threads.

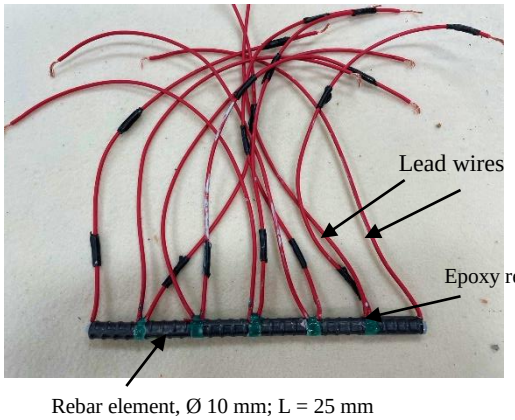

Figure 2 (a). Special divided with six elements soldered with lead wires for electrochemical measurements

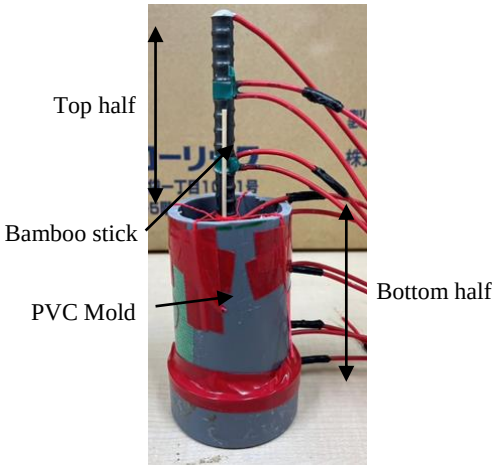

Figure 2 (b). PVC mold for mortar specimen; Bamboo stick to ensure placement of bar

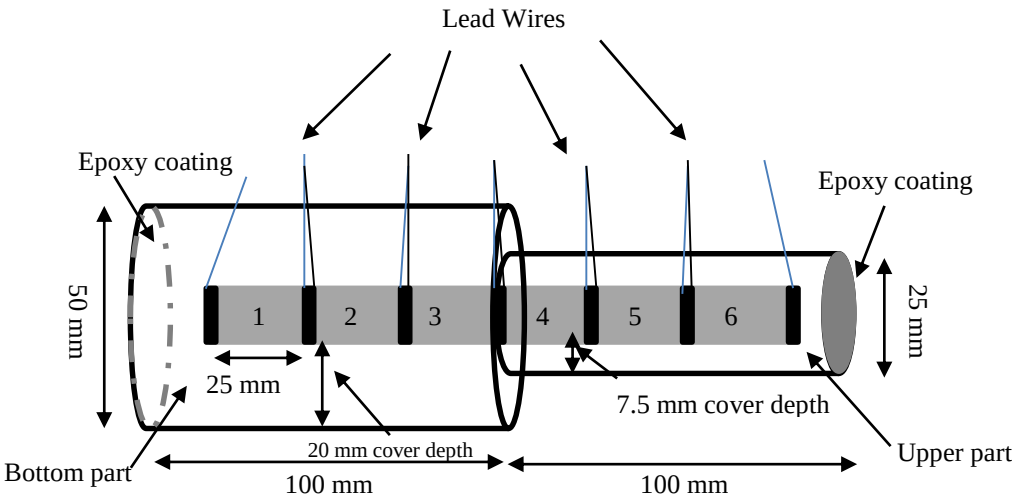

Figure 2 (c). Mortar specimen with partial cover thickness

2.1.2. Material Properties

Ordinary Portland cement (OPC) (JIS R 5210) with a density of 3.16 g/cm^3 and a specific surface area of 3290 cm^2/g, and natural sand with a water absorption of 2.23%, max grain size of 5 mm, and fineness modulus and relative density of 3.22 and 2.52, respectively, were used. Mortar was used because of its homogeneous matrix to avoid heterogeneity in concrete owing to other materials and serves as basic research for concrete. Tap water was used to prepare the mortar mixtures. A 200 mm long cylindrical specimen was cast with a mortar having a W/C of 0.50, as shown in Figure 2 (c). The bottom part of these specimens was cast with a control mixture with a W/C of 0.50 and a diameter of 50 mm to maintain a uniform cover depth of 20 mm. In contrast, the upper part was cast with a mortar mixture of 0.50 CM2.5 containing 2.5 kg/m^3 chloride ion (Cl^-) by volume of mortar with a nominal diameter of 25 mm to establish a cover depth of 7.5 mm. The quantity of chloride ions was added to 0.50 CM2.5 by mixing natural salt (NaCl) in water during kneading. The bottom half of the specimen was cast with 0.50 CM for one day, while the second half was cast with 0.50 CM2.5 within 24 hours with the intention of ensuring proper bonding. On the third day, the specimen was demolded. Consequently, epoxy was applied to the specimens at the top and bottom to prevent the penetration of oxygen, as shown in Figure 2(c). The details of the mix proportions are presented in Table 1. All the specimens were cured inside a curing room while inside a container at 20 ± 2℃ and relative humidity (RH) ≥ 95% for 27 days.

Table 1. Mortar Mix proportions

Symbol (W/C&Cl^-)	S/C	Unit weight (kg/m^3)			
		Water (W)	Cement (C)	Sand (S)	NaCl
0.50CM/0.50CM2.5	2.5	276	553	1384	0/15

2.1.3. Experimental Cases

Two types of inorganic surface penetrants were used: silane/siloxane silicone-based penetrants described as "hydrophobic impregnation (H)" and sodium silicate-based penetrants described as "impregnation (I)" in EN 1504-2. The JSCE guidelines for silane were published in 2005 [44], while those for silicate penetrants were published in 2012 [40]. Both the penetrants were applied with a brush, and the recommended quantity by the manufacturer was used, as shown in Table 2. After curing the specimens for 27 days, they were air dried at RH = 60% and 20 °C for 7 days. As recommended by the manufacturer, the surface moisture was measured every day, and at a surface moisture of 6–7%, the penetrants were applied to the specimens. A silane-based penetrant was applied to the specimens by brushing at 200 g/m^2 and air-dried for 24 h. A sodium silicate-based penetrant was applied with a brush at 240 g/m^2 and air dried for 1 hour, as recommended by the manufacturer. Three specimens (03) were coated with each penetrant according to standard methods. The performances of the coated and uncoated mortar specimens were compared. After setting the penetrants, both the coated and uncoated specimens were cured for 27 days at 20 ± 2 °C and RH ≥ 95%. The experimental cases and the recommended dosage of the penetrants are shown in Table 2.

Table 2. Experimental cases

Case	Classification	Recommended quantity (g/m^2)	Application method	No. of specimen
Silane	Silane/siloxane silicone-based	200	Brush	03
Silicate	Sodium silicate-based	240	Brush	03
Uncoated	No coating	-	No application	03

2.2. Methods

2.2.1. Electrochemical Methods

2.2.1.1. Macrocell Corrosion Current Density

A zero-resistance shunt ammeter (ZRA) was connected between the lead wires of adjacent steel elements, and the electric current was measured. The experimental setup is illustrated in Figure 3. The corrosion current density of the target steel element was calculated using Equation 1, where the sum of the adjacent steel elements was divided by the surface area of the individual element. This provides the macrocell corrosion current density of a single steel element. [18, 45]. The positive values of the macrocell corrosion current density are anodic macrocells, whereas the negative values of the macrocell are the cathodic macrocell corrosion current density.

$$a_{i=} \frac{A_{i-1,i} + A_{i+1,i}}{s_i} \quad (1)$$

where s_i is the surface area of the steel element-i (cm^2), $A_{i-1,i}$ is the macrocell corrosion current for the adjacent steel elements from $i-1$ *to* i (μA), and a_i is the macrocell corrosion current density of the steel element, i ($\mu A/cm^2$).

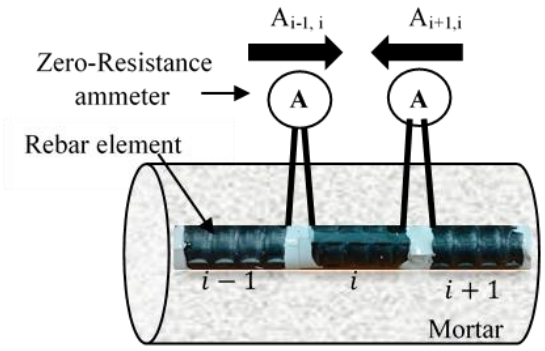

Figure 3. Schematic setup of macrocell current density measurement.

2.2.1.2. Electrical Resistivity

The capacity of a material to withstand electrical circulation is called resistivity [47]. The lead wires were disconnected after the macrocell corrosion current-density test was performed. The lead wires of steel element no. 02 (Figure 2(c)) were connected to the terminal of the ohm meter, those of steel element No. 05 were connected to another terminal, and the surface resistivity was measured in kΩ, as shown in Figure 4.

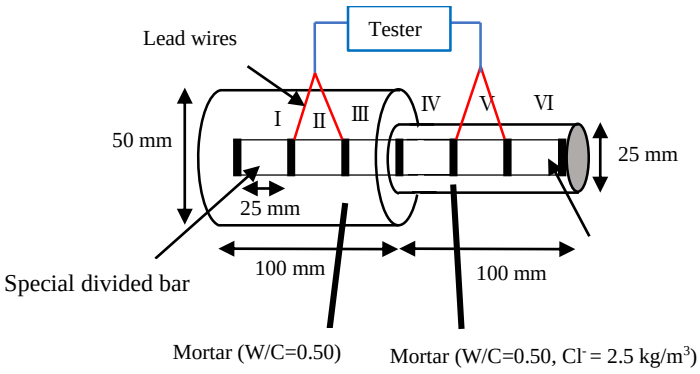

Figure 4. Experimental setup for measurement of electrical resistance of specimen

2.2.1.3. Microcell Corrosion Current Density

A three-electrode system was used to measure the polarization resistance of the steel surface. For each individual steel element embedded in the mortar, as shown in Figure 2(c), as the working electrode, lead wires were connected to the potentiostat of the computer-controlled corrosion monitor. The target steel element was surrounded by a stainless-steel plate surrounded by wet tissue or gel that served as a counter electrode, and Ag/AgCl served as the reference electrode [45, 47-52]. The polarization resistance of each element was determined using the AC impedance method with a frequency-response analyzer (FRA). The current flowing through the individual steel elements was the microcell current density. The experimental setup is shown in Figure 5. The alternating voltage range was ±50 mV with a frequency range of 5 kHz to 5 mHz. The polarization resistance (R_{pi}) for steel element i was obtained as the difference between the total resistance (R_t) and the mortar resistance (R_s) calculated from the Nyquist and Bode diagrams. The polarization resistance was converted by using Equation 2 [47] into microcell corrosion current density.

$$b_i = \frac{k}{R_{pi} \times S_i} \quad (2)$$

where R_{pi} is the polarization resistance ($\Omega.cm^2$), the value of K is constant (0.0209 V), as proposed by Tsuru et al. (1979) [53], b_i is the steel element, and i ($\mu A/cm^2$) is the microcell corrosion current density.

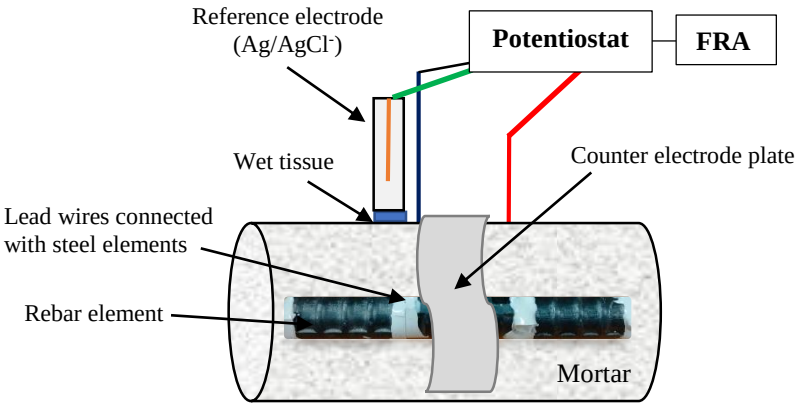

Figure 5. Schematic setup of measurement of polarization resistance

2.2.1.4. Maximum Total Corrosion Current Density

The total corrosion current density of a single steel element is the sum of the anodic macrocell current of a single element measured in Section 2.2.1.1 and the microcell current for the same element calculated from the polarization resistance in Section 2.2.1.3. [17, 18].

2.2.1.5. Potentiodynamic Polarization Curves (PPCs)

The susceptibility of different iron alloys to localized corrosion in a chlorine atmosphere was assessed using the ASTM standard G61-86. A computer-controlled potentiostat with a three-electrode system was used to plot anodic and cathodic polarization curves. Ag/AgCl was used as the reference electrode, as shown in Figure 6 [54]. A potential as applied at a rate of 1 mV/s to the rebar element, and the flowing current was measured. Anodic and cathodic polarization curves were plotted for steel element No. 5 of the coated and uncoated specimens to measure and evaluate the performance of the specimens coated and the uncoated specimen.

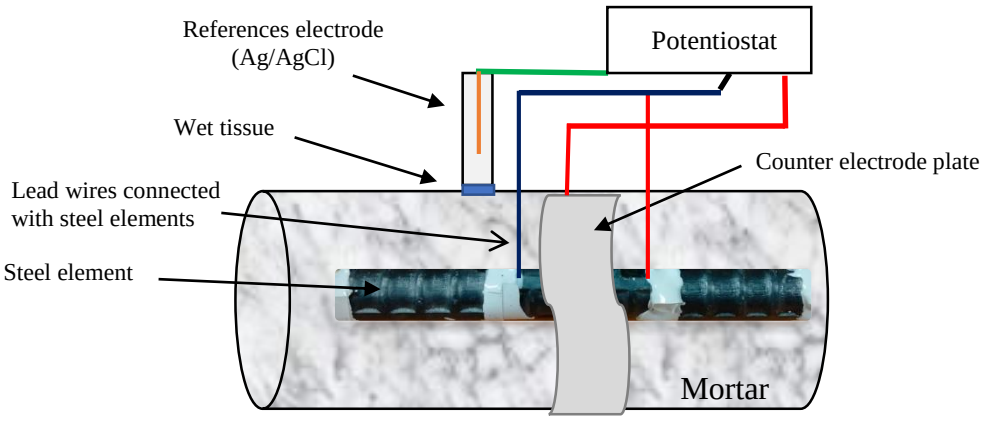

Figure 6. Schematic setup of the polarization curve measurement

2.2.2. Penetration Depth Measurement

2.2.2.1. Silane-based Penetrant

In the case of silane-based penetrant, the specimens were cured for 27 days at a relative humidity (RH) of 95% and 20 ± 2℃. The penetration depth was measured in accordance with JSCE 2005 [55] and applied in accordance with JSCE-K 571. The specimens were gently broken into two pieces and water was sprayed on the split planes. For each specimen, at three locations on both sides of the circular specimens, the depth of the silane-based penetrant was measured from the portion that repelled water, as shown in Figure 7. The average depth of the three points of each specimen and the average of the three specimens were considered in this study [27]. The penetration depth at the locations of the lead wires was greater owing to the passage provided by the lead wires; however, it was not considered in the measurement. The average penetration depth of the silane-based penetrant was 2.76 mm. This confirmed the modification of the substrate surface, as shown in Figure 7.

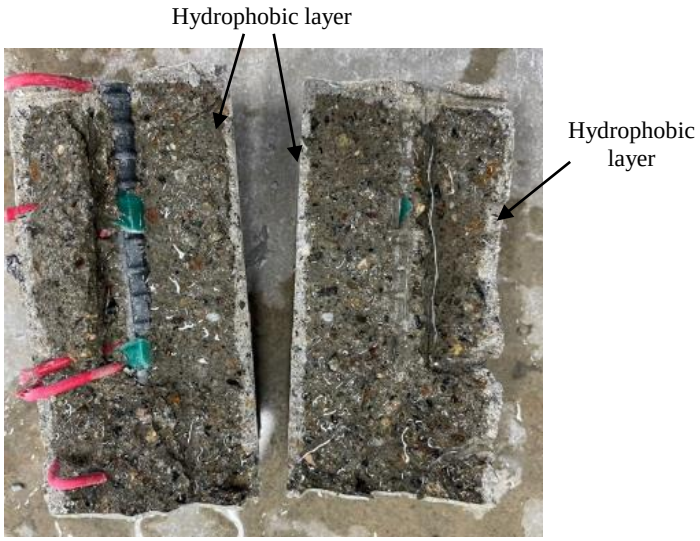

Figure 7. Water-repellent layer due to application of silane penetrant

2.2.2.2. Silicate-based Penetrant

The silicate-based penetrant reacts to form a dense C-S-H gel, which enhances the hardness of the reformed part. In this study, the Vickers hardness (HV) was used to distinguish between the reformed and non-reformed depths of the specimen. Kondo et al. (2023) used the HV test as an index to quantitatively evaluate the reformed and non-reformed parts owing to the application of silicate-based surface penetrants [56].

The HV test was used to measure the hardness of the reformed and non-reformed parts in accordance with JIS Z 2244 [57] using the apparatus shown in Figure 8(a). A 10–15 mm specimen was extracted from the specimen coated with a silicate-based penetrant. The specimens were then subjected to a force of 0.098 N for a retention period of 10

s. Thirty readings were taken randomly at 1 mm intervals from the surface along the depth of the specimen up to 10 mm. At each millimeter, an average of 10 similar readings was recorded to obtain one point on the graph of HV versus depth from the surface (mm) [58]. By evaluating the results of the HV test, the penetration depth of the silicate-based surface penetrant was found to be 4 mm when the hardness of the reformed depth changed, as shown in Figure 8(b).

Figure 8 (a). Vicker's Hardness Test apparatus

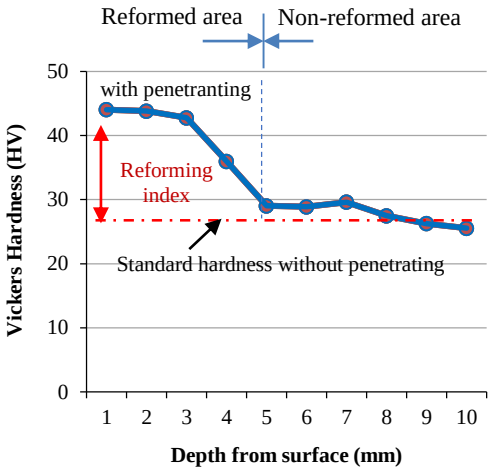

Figure 8 (b). Vickers hardness distribution for specimen coated with silicate-based surface penetrant

3. Experimental Results and Discussions

The influence of the penetrants on the corrosion onset in the chloride environment with a partial short cover depth was investigated using macrocell, microcell, total corrosion current densities, and polarization curves. Three (03) specimens of each penetrant (Section 2.1.2) and three (03) uncoated mortar specimens were tested 28 days before coating and 28 days after coating.

3.1. Electrochemical Measurements

3.1.1. Total Corrosion Current Density and Corrosion Rate (V_{corr})

Figures 9(a) and 9(b) show the variation in the macrocell current density, microcell current density, and total corrosion current density along the length of the bar for a range of 0–200 mm for representative samples after the application of penetrants. The corrosion current densities of steel elements 3, 4, and 5 were greater than those of elements 1, 2, and 3, respectively, because of the partially short covers. The full and partial cover thickness with the same chloride ions were compared in a previous study by the author, which revealed an increase in the corrosion current density of more than 50% owing to the partial cover thickness [4]. The macrocell and microcell corrosion current densities calculated from the polarization resistance were evaluated to find the average total corrosion current density of three (03) specimens of each silane and silicate-based penetrants and uncoated specimens at 28 days before coating and again at 28 days after coating, as shown in Figure 10.

The average of the total corrosion current densities 28 days before coating for the uncoated specimens of the steel elements with the highest total corrosion current densities was averaged. The average total corrosion current densities for both the silane and silicate-based penetrant after coating were less than the limit referred to as a low corrosion level [59]. After coating the specimens with silane and silicate-based penetrants, the uncoated and coated specimens were tested again for macrocell and microcell corrosion current densities. Owing to coating of the specimens, after 28 days, the total corrosion current density of the specimens coated with silane-based penetrant reduced from 0.19 to 0.04 uA/cm^2 and for silicate-based penetrant from 0.19 to 0.09 uA/cm^2. However, in the case of uncoated specimens, the average total corrosion current density was 0.19 µA/cm^2, that is, nearly equal to that measured at the age of 28 days before coating. Shen et al. (2019) used silane as a corrosion inhibitor to decrease the corrosion current density against chloride attack and improved the resistivity of concrete [60]. This result is consistent with that of a previous study.

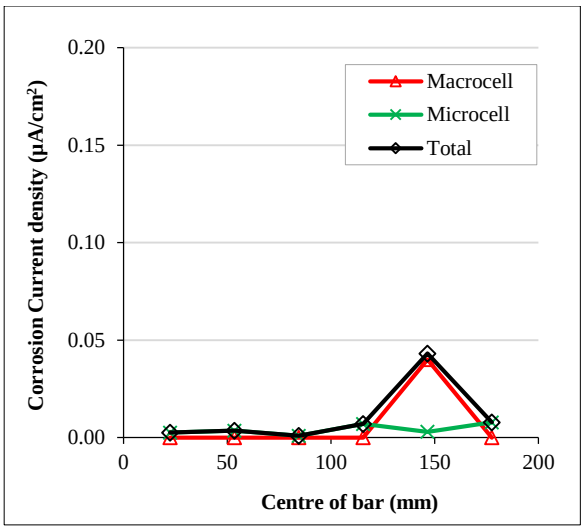

Figure 9(a). Variation in corrosion current density along the length of steel bar after coating with silane-based penetrant.

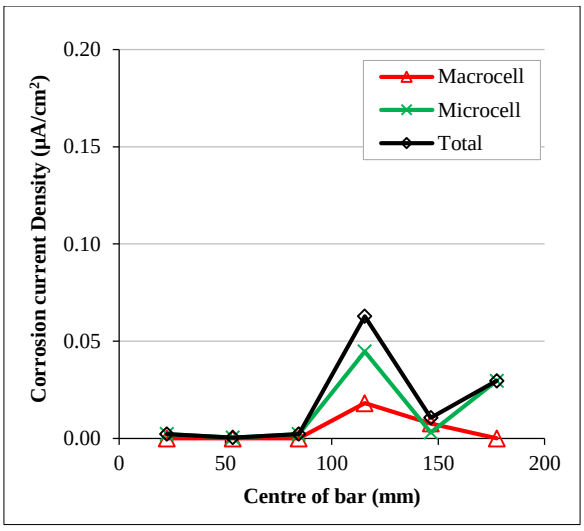

Figure 9(b). Variation in corrosion current density along the length of steel bar with silicate-based penetrant.

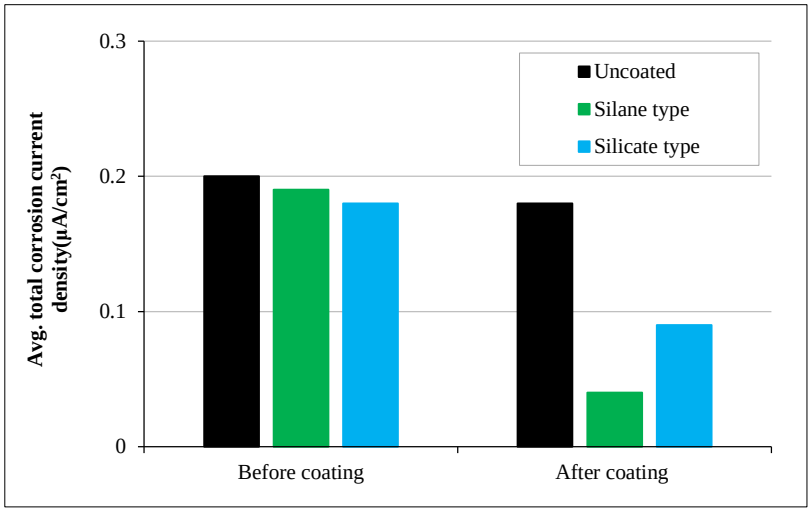

Figure 10. Graph showing the Avg. total corrosion current densities of the specimen before and after coating at the age of 28 days

Vcorr represents the volumetric loss of metal per unit area and time, and I_{corr} represents the corrosion current density [59]. The average values of the total corrosion current densities of the three specimens were substituted into the following equation to obtain the corrosion rate V_{corr} (mm/y) for both the coated and uncoated samples:

$$Corrosion\ rate\ V_{corr}\left(\frac{mm}{y}\right) = \frac{corrosion\ current\ density}{Faraday\ constant} \times \frac{weight\ of\ 1\ mol\ of\ iron}{density\ of\ iron \times 2} \times period \quad (3)$$

$$= \frac{I(A/cm^2)}{96500(C)} \times \frac{55.85(g/mol)}{7.86(g/cm^3) \times 2} \times 10 \times 60(sec) \times 60(min) \times 24(hour) \times 365(day)$$

A comparison of the average corrosion rates V_{corr} (mm/y) at 28 days before coating and 28 days after coating is shown in Figure 11. The values for the coated specimens with both penetrants were in the limit of "no corrosion" as per Rilem recommendations of 2004 [59]. However, for the uncoated specimen, the corrosion rate was relatively high at low-to-moderate corrosion rates. This confirms the influence of both the silicate and silane-based penetrants on the partial cover thickness specimen.

3.1.2. Electric Resistivity

The surface resistivities of uncoated and coated samples were also measured. A comparison of the average electrical resistivity of the three specimens coated with silane and silicate-based penetrants and the uncoated ones is shown in Figure 12. The surface resistivity of the silane-based penetrant was the highest among all the specimens, followed by the silicate-based and uncoated samples. Thus, the performance of the silane-based penetrant is better for resisting the formation of corrosion cells between the anode and cathode, and hence, exhibits a low corrosion rate. Electrical

resistivity is an important factor governing the corrosion process; the higher resistivity of the silane-based penetrant indicates its high resistance to corrosion cell formation [61]. This can also be confirmed from the results of the average corrosion rate V_{corr} in Figure 11, where the corrosion rate of the coated specimen was the lowest among the uncoated and silicate-coated specimens.

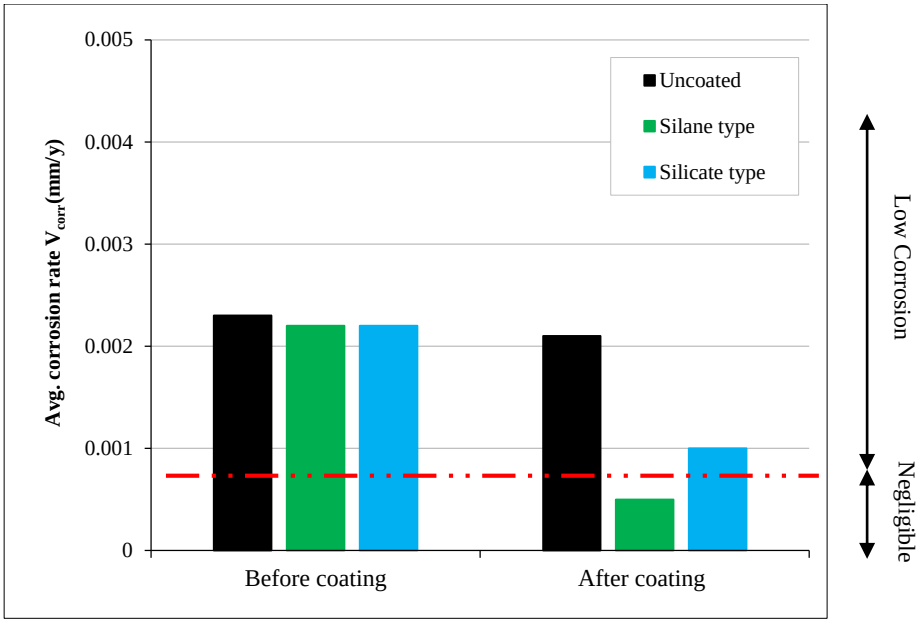

Figure 11. Average corrosion rate V_{corr} (mm/y) for the coated and uncoated specimens at the age of 28 days

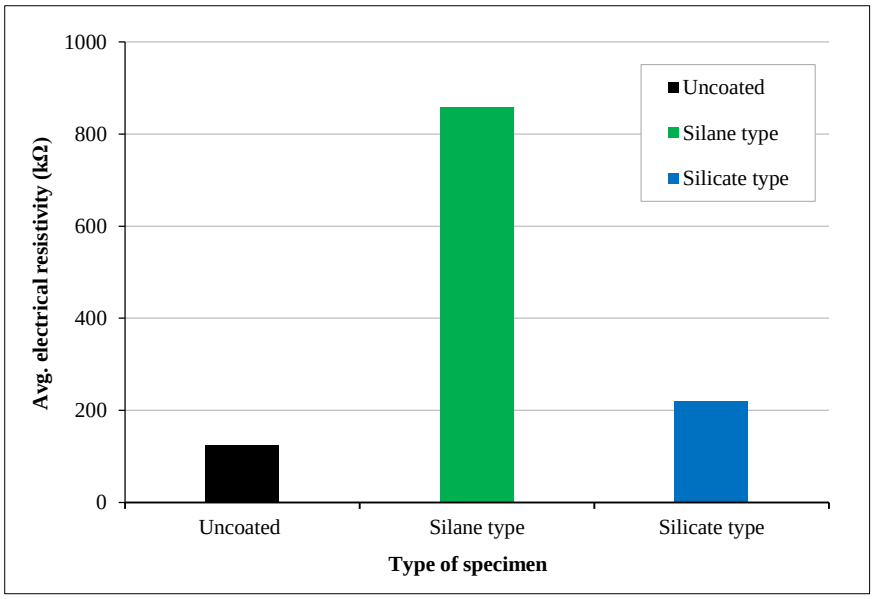

Figure 12. Comparison of average electrical resistivity of 03 specimens for each coated and uncoated specimen.

3.1.3. Polarization Curves

The anodic polarization curves describe the deteriorated status of the passive film owing to the presence of chloride ions [62, 63], whereas the cathodic polarization curves determine the supply of oxygen, temperature, and aging of the passive film [64] in the substrate and the initiation of the cathodic reaction [17]. Figures 13 and 14 show a comparison of the anodic and cathodic polarization curves for the specimens coated with silane and silicate, and the uncoated specimens. The cathodic polarization curves of the silane penetrants confirmed its water repellent property. The anodic and cathodic polarization curves followed the order silane < silicate < uncoated. At every potential, the current density increased in the order: uncoated > silicate > silane. The increase in the current density indicated a higher corrosion rate. Moreover, the tendency of the anodic and cathodic polarization curves for the uncoated sample towards the right side indicated rapid corrosion initiation. However, the curves of the coated specimens towards the left exhibited a low corrosion rate and delayed anodic reaction.

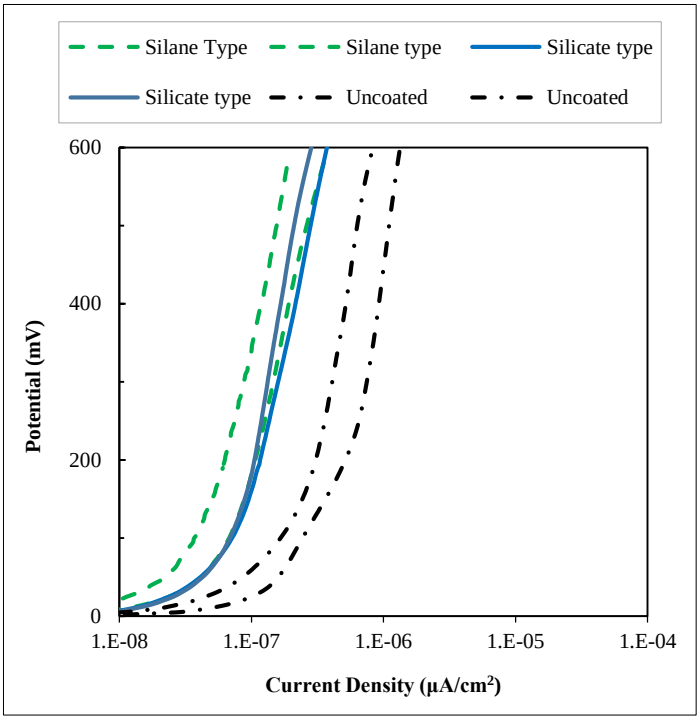

Figure 13. Anodic Polarization curve for the specimens coated with silane and silicate-based penetrants and uncoated specimens

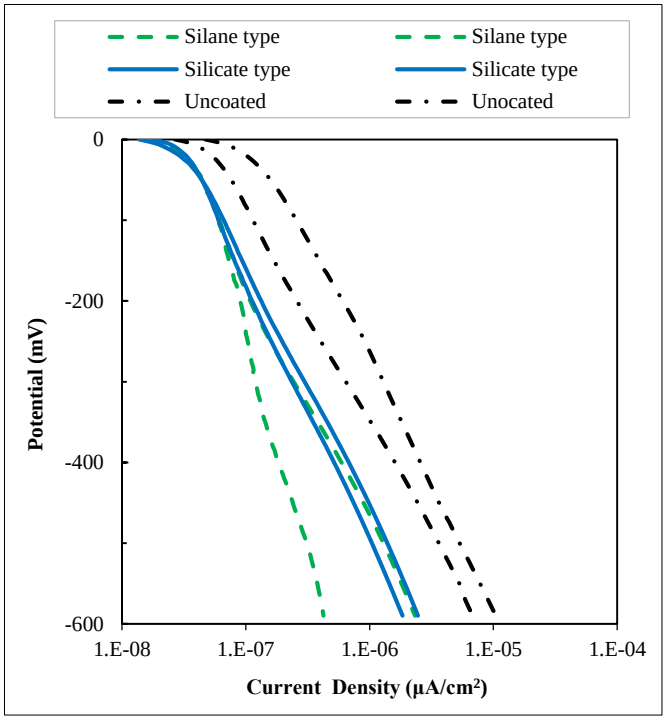

Figure 14. Cathodic Polarization curve for the specimens coated with silane and silicate-based penetrant and uncoated specimens

4. Calculated Results and Discussions

4.1. Equivalent Cover Depth Method

The diffusion of chloride ions into the surface treated with penetrants was evaluated considering two approaches [58, 77]: (a) two-layer model and (b) equivalent cover approach. In this study, an equivalent cover approach was used to evaluate the penetration of chloride ions into the substrate surface. Figure 15 shows a pictorial representation of the equivalent cover approach. The dotted line represents the chloride ion penetration for the mortar surface without treatment (non-reformed part), while the solid curve shows the chloride ion diffusion after the application of the surface penetrants. The equivalent cover depth can be calculated using the following Equation [8]:

$$C_i = C_s \times \frac{\sqrt{D_c}}{\sqrt{D_s}} \quad (4)$$

where C_i is the equivalent cover depth (mm), C_s is the penetration depth (reformed part) (mm), D_s is the apparent diffusion coefficient of the reformed part (cm^2/year), and D_c is the coefficient of diffusion of the non-reformed part (cm^2/year).

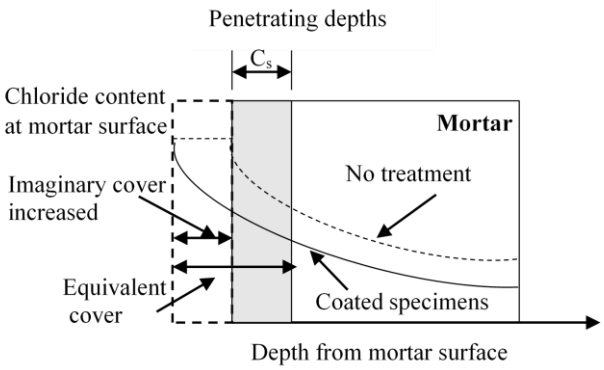

Figure 15. Chloride penetration into a mortar surface with and without application of surface penetrants

A diffusion cell test was performed on specimens coated with the same silane-based surface penetrant at a W/C ratio of 0.50, and the values of the effective diffusion coefficient were obtained from our laboratory [65, 66]. The effective diffusion coefficients were converted to apparent diffusion coefficients using JSCE 2012 [11]. The apparent diffusion coefficient of the silane-based surface penetrant was 0.013 $(cm^2/year)$. Studies have found that, in concrete

impregnated with higher concentration of silane (up to 70%), the apparent diffusion coefficient calculated for the coated specimens was reduced by more than 70% and up to 40% in case of the surface chloride ion content [67]. A study [57] used 12 levels of trial calculations to evaluate the diffusion coefficient for the silicate-based penetrant used in this study, and they concluded that the apparent diffusion coefficient for sodium silicate was 0.56 ($cm^2/year$) for W/C ratio of 50%. The apparent diffusion coefficient of non-reformed part was calculated to be 0.50 ($cm^2/year$) by using the equation recommended by JSCE 2017 for a W/C of 50% [11]. To calculate the equivalent cover depth for each penetrant, the above values of the diffusion coefficients and penetration depths from Section 2.2.2 were substituted into Equation 4. Consequently, the equivalent cover depth of the silane-based surface penetrant was 17.12 mm, whereas that of the silicate was 3.78 mm.

4.2. Service Life Extension Due to Penetrants

4.2.1. Calculation of Converted Cover Depths

In this Section, based on the equivalent cover approach, the service life extension owing to the application of silane and silicate penetrants can be determined. This section presents a structure with W/C of 0.50 and 50 and 70 mm (standard) concrete cover thicknesses at 100 and 250 m from the coastline as a representative case study. The corrosion onset time immediately after construction was calculated for both surface penetrants by using Fick's 2nd law of diffusion. Two standard cover depths of 70 and 50 mm at a distance of 100 and 250 m from the sea coast, respectively, were assumed. In both cases, the corrosion initiation time was calculated for every 5 mm decrease in cover depth. After application of the surface penetrants to the substrate, an impervious layer that helps to prevent penetration of chloride ions and water was formed. As there is difference in diffusion coefficients of penetrants and substrate, this modified part was converted into equivalent cover depth. The converted cover depths for each surface penetrant and short cover are listed in Table 3 based on the equivalent cover depths calculated in Section 4.1. Fick's law of diffusion is expressed as:

$$C(x,t) = C_0\left(1 - erf\frac{x}{2\sqrt{D\cdot t}}\right) \quad (5)$$

where $C(x,t)$ is the chloride ion concentration at depth x (cm) and time t (years) (kg/m^3), C_0 is the surface chloride ion content (kg/m^3), D is the apparent diffusion coefficient (cm^2/year), and erf is the error function.

Table 3. Calculated value of equivalent cover depth after application of penetrants

Distance from coast(m)	Cover depth non reformed part(mm)	Reformed part by Silane-based surface penetrant (mm)	Reformed part by Silicate-based surface penetrant (mm)
100	70	-	-
	60	60+17.12= 77.12	60+3.78=63.78
	50	50+17.12=67.12	50+3.78= 53.78
250	50	-	-
	40	40+17.12 = 57.12	40+3.78 = 43.78
	30	30+17.12 = 47.12	30+3.78 = 33.78

A threshold value of C_{lim} = 1.9 kg/m^3 [8] was used for the total chloride ion concentration around the steel bar. The time (years) required to reach this threshold value was calculated considering the reformed depth identified in Figure 15. The apparent diffusion coefficient of 0.50 cm^2/year was substituted in Equation 5. The values of the surface chloride ions were 3 and 4.5 kg/m^3 for structures 250 and 100 m from the coastline, respectively [60].

4.2.2. Corrosion Onset Time for a Structure at 100 m and 250 m from the Coastline

Figure 16 shows the trial calculation results for the uncoated cover depths of 70, 65, 60, 55, and 50 mm with a decrease of 5 mm [1-3] in cover thickness and converted depths at a distance of 100 m from the coastline using the equivalent cover approach described in Section 4.1. The threshold of the chloride content reached 1.9 kg/m^3 for a 70 mm cover depth in the 76th year, 66th year for 65 mm, 56th year for 60 mm, 47th year for 55 mm, and 39th year for 50 mm using Equation 5 for uncoated structures under the non-corrosion performance requirement. The average decrease in corrosion initiation time was calculated to be 10 years for a 5 mm decrease in cover depth.

The application of a silane-based penetrant extended the corrosion onset time from the 66th to 104th year for 65 mm, 56th to 92nd year for 60 mm, 47th to 80th year for 55 mm, and 39th to 70th year for a 50 mm cover depth. However, the silicate-based penetrant extended the corrosion onset time from the 66th to 73rd year for 65 mm, 56th to 63rd year for 60 mm, 47th to 54th year for 55 mm, and 39th to 45th year for a 50 mm cover depth.

For a 5 mm decrease in cover depth from the original 70 to 65 mm, the application of a silicate-based penetrant increased the corrosion initiation time to 73 years (almost equal to 76 years). The silane-based penetrant was effective

even for a short cover depth of 50 mm and could increase the corrosion initiation period up to 70 years, which is equivalent to the actual corrosion initiation period of 76 years. Hence, a silicate-based penetrant can only be used for a structure at a 100 m coastline with a 5 mm deficient cover from the original cover depth, whereas a silane-based penetrant can be used even for treating a deficient cover depth up to 20 mm from the original cover depths at 100 m from the coastline.

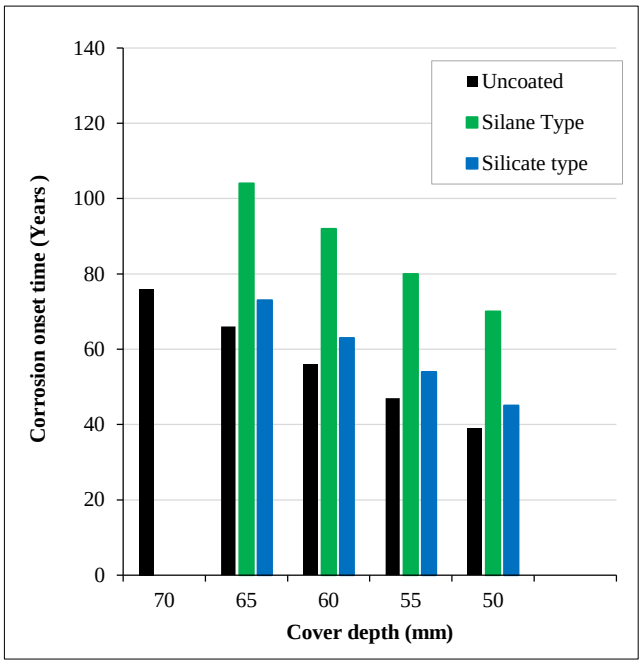

Figure 16. Trial calculations results for a structure located at 100 m from the coastline

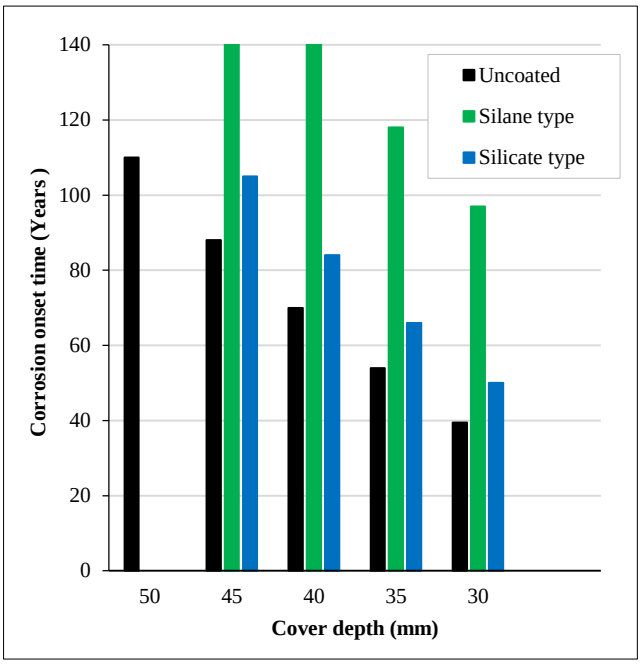

Figure 17. Trial calculations results for a structure located at 250 m from the coastline

Figure 17 shows the trial calculation results for the uncoated cover depths of 50, 45, 40, 35, and 30 mm with a decrease of 5 mm cover depth, and the converted depths for each corresponding converted depth at a distance of 250 m from the coastline using the equivalent cover approach described in Section 4.1. The threshold of the chloride content reached 1.9 kg/m^3 for a 50 mm cover depth in the 110th year, 88th year for 45 mm, 70th year for 40 mm, 54th year for 35 mm, and 39th year for 30 mm using equation 5 for uncoated structures under non-corrosion performance requirements. The average decrease in the corrosion initiation time was calculated 15–22 years for a 5 mm decrease in cover depth.

The application of a silane-based penetrant extended the corrosion onset time for 45, 40, and 35 mm cover depths to more than the original corrosion onset time for a 50 mm cover depth without coating. Even in the case of a 30 mm short cover depth, the corrosion onset time was calculated to be almost equal to that of the design period of bridges in Japan. The silane penetrants for higher W/C ratio of 0.50 and 0.65 can be applied to new structures at an earlier age to obtain much more water-repellent effect [27]; previous study confirmed the application of silane-based penetrant to new structures. The silane-based penetrant was applied to existing structures after 10 years of service life, and the diffusion coefficient was considered, half of the actual diffusion coefficient of the mortar. The silane penetrant performed well in comparison with the sodium silicate-based penetrant in extending the service life of structures [65]. These results are consistent with those of the present study. Silane/nanocomposites enhanced the barrier properties of concrete against salt-frost scaling and physical salt attack (PSA) [68].

However, the silicate penetrant extended the corrosion onset time from the 88th to 105th year for 45 mm, 70th to 84th year for 40 mm, 54th to 66th year for 35 mm, and 39th to 50th year for a 30 mm cover depth. For a decrease of 5 mm, the silicate penetrant was effective in extending the corrosion onset time to be equivalent to the original time for a 50 mm cover depth. The silane-based penetrant was effective even for a short cover depth of 30 mm and increased the corrosion initiation period up to the 97th year, which is equivalent to an actual corrosion initiation period of 100 years. Hence, a silicate-based penetrant can only be used for a structure at a 250 m coastline with a 5 mm deficient cover from the original cover depth. Research reports that silicate-based penetrant was effective at a distance of 500 m for a cover depth of 50 mm in prolonging the service life by 9-12 years [57], which is consistent with this study. Thus, silicate-based penetrant was only effective for a 5 mm deficient cover than original cover of 50 mm at 250 m from the sea coast. Whereas, silane-based penetrant can be used even for treating deficient cover depths up to 20 mm from the original cover depths at 250 m from the coastline.

4.2.3. Corrosion Weight Loss of Steel at 100 m and 250 m from the Coastline

Concrete cover deteriorates in four main stages: (i) corrosion onset, (ii) corrosion propagation or crack occurrence, (iii) acceleration, and (iv) deterioration [69]. This propagation stage is relatively short compared with the corrosion initiation stage [12-13]. Figure 18 shows the relationship between corrosion weight loss (mg/cm^2) and time in years from corrosion onset to the propagation stage for uncoated covers of 70, 60, and 50 mm for a structure 100 m from the coastline. The results of the corrosion rate V_{corr} (mm/y) of both penetrants from Section 3.1.1 and Figure 11 were converted to the corrosion weight loss (mg/cm^2). A threshold of 10 mg/cm^2 was considered in this study based on the JSCE Maintenance Manual for the occurrence of longitudinal corrosion cracks [70, 71].

The slopes of the silane penetrant for the 60 and 50 mm cover depths show a delayed occurrence of longitudinal corrosion cracks. This delay was attributed to the corrosion rate of 0.0005 mm/year for the specimen coated with the silane penetrant. Unlike silane, the performance of silicate at cover depths of 60 and 50 mm at a distance of 100 m from the coastline did not appear to be good. Figure 19 shows the effect of the silane and silicate penetrants on the corrosion weight loss of steel embedded in concrete at a distance of 250 m from the coastline for cover depths of 40 and 30 mm. The crack occurrence for silane at both cover depths was equal to or greater than 100 years, which is equivalent to the design life of RC structures in Japan. Hence, it can be concluded that if the silane-based penetrant was used for treating the short cover issue as a preventive maintenance strategy, it would be highly effective in prolonging the service life of RC structures near the coastline at distances of 100 and 250 m with a recoating in every 20 years based on a recent study of silane penetrant; its application to actual structures and 20 years of exposure tests for combined degradation due to freeze thaw damage and salt damage for verifying long-term durability, has concluded that the silane penetrant is durable and can withstand up to 20 years [72].

However, certain studies based on uncertainty analysis reported that the service life extension by the application of silane penetrants may be shorter than assumed; therefore, early applications are recommended [73]. Petcherdchoo [74] compared concrete cover replacement and silane treatment for a concrete cover thickness of 30 mm. Silane was applied every 7 years, and the chloride ion content was calculated using the finite difference method; it was concluded that after 100 years, the surface treated with silane had a lower amount of chloride ions.

The effectiveness of the silicate-based penetrant could only be established at a short cover of 5 mm from the design cover at 100 and 250 m from the coastline. Regarding the durability of the surface penetrant is concerned, Kuang et al. [75] evaluated that surface penetrants may be applied at intervals of every 15 years to maintain structures throughout the service life. Miyazaki & Miyazato [42] proposed a maintenance model based on recoating every 20th year of silane penetrant and proposed recoating every 10th year for Silicate penetrant under non-corrosion performance requirement. When calculating the service lives of the structures in this study, the maintenance model proposed in a previous study by the second author was considered [76].

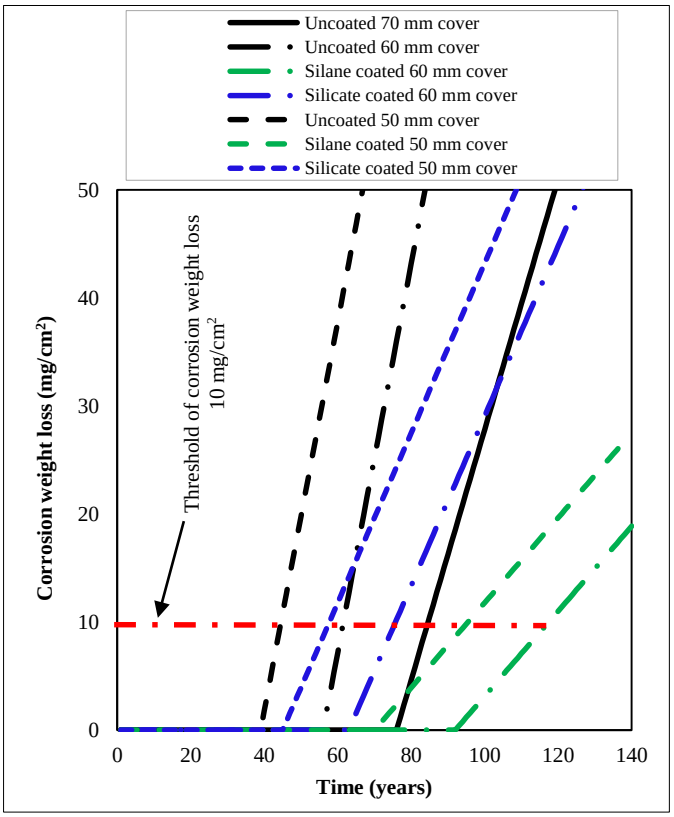

Figure 18. Influence of surface penetrants on corrosion onset and propagation of corrosion up to cracking of concrete cover at 100 m from coastline.

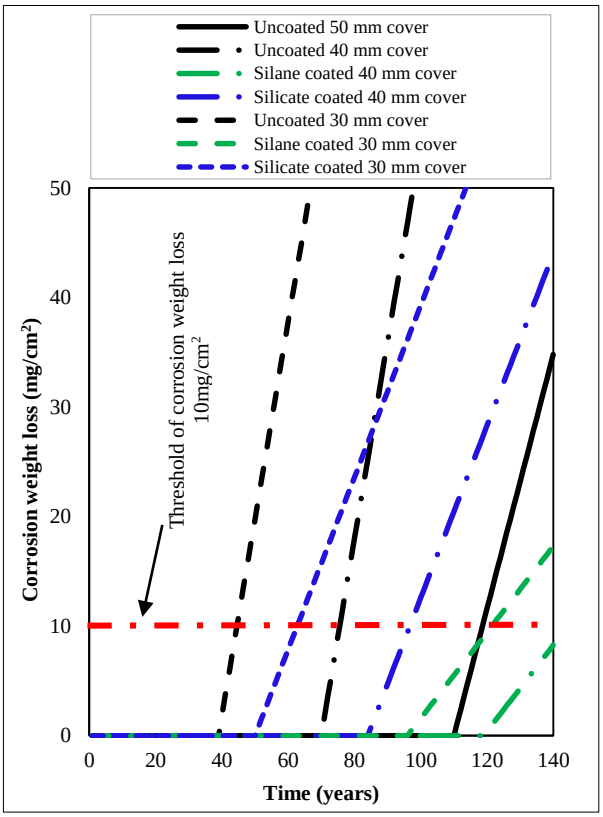

Figure 19. Influence of surface penetrants on corrosion onset and propagation of corrosion up to cracking of concrete cover at 250 m from coastline.

5. Conclusions

In this study, silane and silicate penetrants were quantitatively assessed in terms of their performance against corrosion of steel embedded in a partial cover thickness under a chloride environment. The use of a special segmented bar for localized corrosion is a strength. Based on the determined penetration depths and equivalent cover depths, the corrosion onset and propagation times were calculated for structures with short cover depths at distances of 100 and 250 m from the coastline. The following conclusions were drawn:

- The total corrosion current density of specimens coated with silane decreased by 79% and silicate by 52%, thus indicating the effect of surface penetrants on the corrosion current. The corrosion current densities of the uncoated specimens are similar.
- The average corrosion rate, V_{corr} (mm/y), of the silane-based specimen was 0.0005 mm/y, whereas that of the silicate-based specimen was 0.001 mm/y. Both values were less than 0.001 mm/y, which corresponds to a negligible corrosion rate.
- The electrical resistivity of the specimen coated with the silane-based penetrant was the highest among all specimens, indicating a low corrosion rate. Similarly, for the silicate-based penetrant, the electrical resistivity was higher than that of the uncoated specimens.
- The magnitude of the current density at every potential in the cathodic polarization curves increased in the following order: silane < silicate < uncoated, indicating the cathodic reaction status.
- The silane penetrant was effective in treating deficient cover thicknesses up to a maximum of 20 mm from the typical cover thicknesses of 70 and 50 mm at distances of 100 and 250 m from the coastline, respectively.
- The silicate penetrant was effective in treating the deficient cover thickness up to a maximum of 5 mm from the typical cover thicknesses of 70 and 50 mm at a distance of 100 and 250 m from the coastline.

Based on the significant findings of this study, silane/siloxane penetrants are suitable for delaying the corrosion onset in structures 100 and 250 m from the coastline arising from the partial thickness of the cover. However, silicate penetrants are only applicable up to a deficient cover of 5 mm at 100 and 250 m from the coastline. Field engineers may opt for silane and silicate penetrants based on the benefit/cost ratio and the distance of structures from the coastline. This study was limited to mortar specimens with partial cover thicknesses as a basic study of concrete. However, based on the findings of this study, more extensive field studies are recommended to support the use of laboratory tests.

6. Declarations

6.1. Author Contributions

Conceptualization, K.M.A. and M.S.; methodology, experimentation, K.M.A., M.T., and M.H.; writing—original draft preparation, K.M.A.; writing—review and editing, K.M.A.; supervision, M.S.; project administration, M.S. All authors have read and agreed to the published version of the manuscript.

6.2. Data Availability Statement

The data presented in this study are available in the article.

6.3. Funding

This study was supported financially by the Japan International Cooperation Agency (JICA).

6.4. Acknowledgements

The authors are grateful to Kajima Renovate Co. Ltd. for providing samples of the silane-based penetrant and Fuji Chemical Co. Ltd. for providing the sodium silicate-based penetrant. The support of the Japan International Cooperation Agency (JICA) is gratefully acknowledged throughout this study.

6.5. Conflicts of Interest

The authors declare no conflict of interest.

7. References

[1] ACI-117-10. (2010). Specification for Tolerances for Concrete Construction and Materials (ACI 117-10) and Commentary. ACI Committee, American Concrete Institute, Indiana, United States, 1–76.

[2] BS EN 206-1 (2012). Concrete – Complementary British Standard to BS EN 206-1 – Part 2: Specification for constituent materials and concrete. British Standards Institution (BSI), London, United Kingdom.

[3] JSCE (2007). Standard Specifications for Concrete Structures. JSCE Guidelines for Concrete No. 15, Tokyo, Japan.

[4] Muhammad, A. K, Miyazato, S., and Sugawara, N. (2023). Influence of Cover depth and mortar quality on Rebar corrosion under aggressive chloride environment". Proceedings of the 4th Asian Concrete Federation symposium on emerging technologies for structural longevity (ACF2023_ETSL), Shenzhen, China.

[5] ABNT NBR. 6118. (2014). Projeto de Estruturas de Concreto–Procedimento. Rio de Janeiro, Brazil, 238.

[6] Petcherdchoo, A. (2016). Pseudo-coating model for predicting chloride diffusion into surface-coated concrete in tidal zone: Time-dependent approach. Cement and Concrete Composites, 74, 88–99. doi:10.1016/j.cemconcomp.2016.08.009.

[7] Liang, Y., & Wang, L. (2020). Prediction of corrosion-induced cracking of concrete cover: A critical review for thick-walled cylinder models. Ocean Engineering, 213, 107688. doi:10.1016/j.oceaneng.2020.107688.

[8] Baroghel-Bouny, V. (2007). Concrete design for a given structure service life: durability management with regard to reinforcement corrosion and alkali-silica reaction: state of the art and guide for the implementation of a predictive performance approach based upon durability indicators. Association Française de Génie Civil, Paris, France.

[9] Bentur, A., Diamond, S., & Berke, N. S. (1997). Steel corrosion in concrete : fundamentals and civil engineering practice. CRC Press, Florida, United States.

[10] Truong, Q. C., El Soueidy, C. P., Li, Y., & Bastidas-Arteaga, E. (2022). Probability-based maintenance modeling and planning for reinforced concrete assets subjected to chloride ingress. Journal of Building Engineering, 54, 104675. doi:10.1016/j.jobe.2022.104675.

[11] JSCE (2012). Standards specifications for Design. Japan society for Civil Engineers (JSCE), Tokyo, Japan. Available online: https://www.jsce-int.org/about/guideline (accessed on June 2023).

[12] Ma, Y., Guo, Z., Wang, L., & Zhang, J. (2017). Experimental investigation of corrosion effect on bond behavior between reinforcing bar and concrete. Construction and Building Materials, 152, 240–249. doi:10.1016/j.conbuildmat.2017.06.169.

[13] Bastidas-Arteaga, E., El Soueidy, C. P., Amiri, O., & Nguyen, P. T. (2020). Polynomial chaos expansion for lifetime assessment and sensitivity analysis of reinforced concrete structures subjected to chloride ingress and climate change. Structural Concrete, 21(4), 1396–1407. doi:10.1002/suco.201900398.

[14] Khalid, M. A., Miyazato, S., Mizuguchi, H., & Miyaguchi, K. (2023). Performance Evaluation of Lithium Nitrite-Based Gel against Corrosion of Rebar with Partial Short Cover Depth in Chloride Environment. Engineering Proceedings, 55(1), 35. doi:10.3390/engproc2023055035.

[15] Gu, X., Dong, Z., & Jin, Z. (2018). Macrocell corrosion between crossed steel rebars embedded in concrete under chloride environments. MATEC Web of Conferences, 199, 04005. doi:10.1051/matecconf/201819904005.

[16] Hansson, C. M., Poursaee, A., & Laurent, A. (2006). Macrocell and microcell corrosion of steel in ordinary Portland cement and high performance concretes. Cement and Concrete Research, 36(11), 2098–2102. doi:10.1016/j.cemconres.2006.07.005.

[17] Chen, L., & Su, R. K. L. (2021). Corrosion rate measurement by using polarization resistance method for microcell and macrocell corrosion: Theoretical analysis and experimental work with simulated concrete pore solution. Construction and Building Materials, 267, 121003. doi:10.1016/j.conbuildmat.2020.121003.

[18] Miyazato, S., & Otsuki, N. (2022). Measurement Method for Macrocell Corrosion in Concrete Specimen using a Segmented Steel Bar. Journal of Advanced Concrete Technology, 20(3), 222–235. doi:10.3151/jact.20.222.

[19] Xian, Y. Z., Wittmann, F. H., Zhao, T. J., & Giessler, S. (2007). Chloride penetration into integral water repellent concrete/eindringen von chloriden in integral hydrophobierten beton. Restoration of Buildings and Monuments, 13(1), 17-24. doi:10.1515/rbm-2007-6103.

[20] Freitag, S. A., & Bruce, S. M. (2010). The influence of surface treatments on the service lives of concrete bridges. Wellington, NewZealand: New Zealand Transport Agency.

[21] Pan, X., Shi, Z., Shi, C., Ling, T. C., & Li, N. (2017). A review on concrete surface treatment Part I: Types and mechanisms. Construction and Building Materials, 132, 578–590. doi:10.1016/j.conbuildmat.2016.12.025.

[22] Schueremans, L., Van Gemert, D., & Giessler, S. (2007). Chloride penetration in RC-structures in marine environment - Long term assessment of a preventive hydrophobic treatment. Construction and Building Materials, 21(6), 1238–1249. doi:10.1016/j.conbuildmat.2006.05.006.

[23] Christodoulou, C., Goodier, C. I., Austin, S. A., Webb, J., & Glass, G. K. (2013). Long-term performance of surface impregnation of reinforced concrete structures with silane. Construction and Building Materials, 48, 708–716. doi:10.1016/j.conbuildmat.2013.07.038.

[24] Zhan, H., & Wittmann, F. H. (2014). Relation between the Silicon Resin Profiles in Water Repellent Treated Concrete and the Effectiveness as a Chloride Barrier. Restoration of Buildings and Monuments, 11(1), 35–46. doi:10.1515/rbm-2005-5926.

[25] Dai, J., Akira, Y., Yokota, H., & Wittmann, F. H. (2014). Surface Impregnation of Pre-conditioned Concrete Subjected to Seawater Immersion Test. Restoration of Buildings and Monuments, 13(4), 229–240. doi:10.1515/rbm-2007-6141.

[26] Zhang, P., Shang, H., Hou, D., Guo, S., & Zhao, T. (2017). The Effect of Water Repellent Surface Impregnation on Durability of Cement-Based Materials. Advances in Materials Science and Engineering, 2017. doi:10.1155/2017/8260103.

[27] Hosoda, A., Matsuda, Y., & Kobayashi, K. (2010). Optimum surface protection system with silane type water repellents. Journal of Advanced Concrete Technology, 8(3), 291–302. doi:10.3151/jact.8.291.

[28] Zhao, J., Gao, X., Chen, S., Lin, H., Li, Z., & Lin, X. (2022). Hydrophobic or superhydrophobic modification of cement-based materials: A systematic review. Composites Part B: Engineering, 243, 110104. doi:10.1016/j.compositesb.2022.110104.

[29] Liu, G., Gjørv, O. E., & Årskog, V. (2010). Effect of concrete surface hydrophobation against chloride penetration. Concrete under Severe Conditions: Environment and Loading - Proceedings of the 6th International Conference on Concrete under Severe Conditions, CONSEC'10, 2, 1157–1163. doi:10.1201/b10552-152.

[30] Jones, M. R., Dhir, R. K., & Gill, J. P. (1995). Concrete surface treatment: Effect of exposure temperature on chloride diffusion resistance. Cement and Concrete Research, 25(1), 197–208. doi:10.1016/0008-8846(94)00127-K.

[31] Basheer, P. A. M., Basheer, L., Cleland, D. J., & Long, A. E. (1997). Surface treatments for concrete: Assessment methods and reported performance. Construction and Building Materials, 11(7–8), 413–429. doi:10.1016/S0950-0618(97)00019-6.

[32] Ibrahim, M., Al-Gahtani, A. S., Maslehuddin, M., & Dakhil, F. H. (1999). Use of Surface Treatment Materials to Improve Concrete Durability. Journal of Materials in Civil Engineering, 11(1), 36–40. doi:10.1061/(asce)0899-1561(1999)11:1(36).

[33] Ibrahim, M., Al-Gahtani, A. S., Maslehuddin, M., & Almusallam, A. A. (1997). Effectiveness of concrete surface treatment materials in reducing chloride-induced reinforcement corrosion. Construction and Building Materials, 11(7–8), 443–451. doi:10.1016/s0950-0618(97)00023-8.

[34] Sivasankar, A., Arul Xavier Stango, S., & Vedalakshmi, R. (2013). Quantitative estimation on delaying of onset of corrosion of rebar in surface treated concrete using sealers. Ain Shams Engineering Journal, 4(4), 615–623. doi:10.1016/j.asej.2013.01.007.

[35] Courard, L., Zhao, Z., & Michel, F. (2021). Influence of hydrophobic product nature and concentration on carbonation resistance of cultural heritage concrete buildings. Cement and Concrete Composites, 115, 103860. doi:10.1016/j.cemconcomp.2020.103860.

[36] Dai, J. G., Akira, Y., Wittmann, F. H., Yokota, H., & Zhang, P. (2010). Water repellent surface impregnation for extension of service life of reinforced concrete structures in marine environments: The role of cracks. Cement and Concrete Composites, 32(2), 101–109. doi:10.1016/j.cemconcomp.2009.11.001.

[37] Li, J., Yi, Z., & Xie, Y. (2012). Progress of silane impregnating surface treatment technology of concrete structure. Mater. Rev, 26(3), 120-125. doi:10.3969/j.issn.1005-023X.2012.03.024.

[38] Moon, H. Y., Shin, D. G., & Choi, D. S. (2007). Evaluation of the durability of mortar and concrete applied with inorganic coating material and surface treatment system. Construction and Building Materials, 21(2), 362–369. doi:10.1016/j.conbuildmat.2005.08.012.

[39] Kupwade-Patil, K., Cardenas, H. E., Gordon, K., & Lee, L. S. (2012). Corrosion Mitigation in Reinforced Concrete Beams via Nanoparticle Treatment. ACI Materials Journal, 109(6), 617-626. doi:10.14359/51684159.

[40] Deng, G., He, Y., Lu, L., Wang, F., & Hu, S. (2023). A preliminary study on the efficiency of the steel slag-based spraying carbonation layer in improving the durability of cement-based products. Cement and Concrete Composites, 136, 104899. doi:10.1016/j.cemconcomp.2022.104899.

[41] Franzoni, E., Pigino, B., & Pistolesi, C. (2013). Ethyl silicate for surface protection of concrete: Performance in comparison with other inorganic surface treatments. Cement and Concrete Composites, 44, 69–76. doi:10.1016/j.cemconcomp.2013.05.008.

[42] Miyazaki, Y., & Miyazato, S. (2018). Permeability of mortar with surface penetrant after weathering test for 20 years. Proceedings of Proceedings of Repair, Reinforcement, and Upgarding of Concrete Structures, Japan.

[43] Hazehara, H., Soeda, M., & Hashimoto, S. (2015). Fundamental study on characteristics of silicate based surface penetrants and effects of improvement on concrete structures. Life-Cycle of Structural Systems: Design, Assessment, Maintenance and Management - Proceedings of the 4th International Symposium on Life-Cycle Civil Engineering, IALCCE 2014, 2014, 971–978. doi:10.1201/b17618-141.

[44] Miyazato, S. I., & Otsuki, N. (2010). Steel corrosion induced by chloride or carbonation in mortar with bending cracks or joints. Journal of Advanced Concrete Technology, 8(2), 135–144. doi:10.3151/jact.8.135.

[45] Padilla, V., & Alfantazi, A. (2014). Corrosion film breakdown of galvanized steel in sulphate–chloride solutions. Construction and Building Materials, 66, 447-457. doi:10.1016/j.conbuildmat.2014.05.053.

[46] Lataste, J. F., Villain, G., & Balayssac, J. P. (2018). Electrical methods. Non-destructive Testing and Evaluation of Civil Engineering Structures, 139-172. doi:10.1016/B978-1-78548-229-8.50004-2.

[47] Stern, M., A. L. G. (1957). Electrochemical Polarization: I. A Theoretical Analysis of the Shape of Polarization Curves. Journal of the Electrochemical Society, 104(1), 56.

[48] Andrade, C., & González, J. A. (1978). Quantitative measurements of corrosion rate of reinforcing steels embedded in concrete using polarization resistance measurements. Materials and Corrosion, 29(8), 515–519. doi:10.1002/maco.19780290804.

[49] Katayama, H. (2014). Surface and interfacial analysis using electrochemical impedance measurement. Nippon Kinzoku Gakkaishi/Journal of the Japan Institute of Metals, 78(11), 419–425. doi:10.2320/jinstmet.JB201402.

[50] Chandra Paul, S. (2018). A Review on Reinforcement Corrosion Mechanism and Measurement Methods in Concrete. Civil Engineering Research Journal, 5(3), 555–661. doi:10.19080/cerj.2018.05.555661.

[51] Andrade, C. (2019). Propagation of Reinforcement Corrosion: Principles, Testing And Modelling. Materials and Structures, 52(1), 2. doi:10.1617/s11527-018-1301-1.

[52] Suryanto, B., Kim, J., McCarter, W. J., Starrs, G., & Aitken, M. W. (2020). Assessing the performance and transport properties of concrete using electrical property Measurements. Journal of Advanced Concrete Technology, 18(7), 437–455. doi:10.3151/JACT.18.437.

[53] Tsuru, T., Maeda, R., & Haruyama, S. (1979). Application of a-C Corrosion Monitor to Localized Corrosion. Boshoku Gijutsu, 28(12), 638–644. doi:10.3323/jcorr1974.28.12_638.

[54] ASTM Standard G61-86. (2010). Standard Test Method for Conducting Cyclic Potentiodynamic Polarization Measurements for Localized Corrosion Susceptibility of Iron, Nickel or Cobalt Based Aalloys. Annual Book of ASTM Standards, 86, G61-86. ASTM International, Pennsylvania, United States.

[55] JSCE-K 572 (2012). JSCE Standards: Test Methods of Silicate-Type Surface Penetrants for Concrete Structures. Japan society for Civil Engineers (JSCE), 68(4), 366-384. doi:10.2208/jscejmcs.68.366.

[56] Kondo, T., Kuroiwa, D., Miyazato, S. I., Shimamura, K., & Takahashii, Y. (2023). Quantitative Evaluation on Reforming Effect of Silicate-based Surface Penetrants Using Vickers Hardness as an Index. Zairyo/Journal of the Society of Materials Science, Japan, 72(7), 507–513. doi:10.2472/jsms.72.507.

[57] Miyazato, S., & Kuroiwa, D. (2014). Determination of chloride ion diffusion coefficient in outer layer of concrete with silicate-type surface penetrant. In G. et.al (Ed.), Concrete Solutions - Proceedings of Concrete Solutions, 5th International Conference on Concrete Repair, Taylor & Francis Group, 409–416. doi:10.1201/b17394-64.

[58] Takewaka, K. (2012). Toward Establishing Recommendations for Silicate-based Surface Impregnation Method for Concrete Structures. Concrete Journal, 50(10), 889-895. doi:10.3151/coj.50.889.

[59] Andrade, C., Alonso, C., Gulikers, J., Polder, R., Cigna, R., Vennesland, Salta, M., Raharinaivo, A., & Elsener, B. (2004). Test methods for on-site corrosion rate measurement of steel reinforcement in concrete by means of the polarization resistance method. Materials and Structures, 37(273), 623–643. doi:10.1617/13952.

[60] Shen, L., Jiang, H., Cao, J., & Zhang, H. (2019). The effect of electro-migrating 3-Aminopropyltriethoxysilane on the improvement of the reinforced concrete durability. Construction and Building Materials, 214, 101–110. doi:10.1016/j.conbuildmat.2019.04.130.

[61] Rodrigues, R., Gaboreau, S., Gance, J., Ignatiadis, I., & Betelu, S. (2021). Reinforced concrete structures: A review of corrosion mechanisms and advances in electrical methods for corrosion monitoring. Construction and Building Materials, 269, 121240. doi:10.1016/j.conbuildmat.2020.121240.

[62] Bertolini, L., & Redaelli, E. (2009). Depassivation of steel reinforcement in case of pitting corrosion: detection techniques for laboratory studies. Materials and Corrosion, 60(8), 608–616. doi:10.1002/maco.200905276.

[63] Song, G. (2000). Theoretical analysis of the measurement of polarization resistance in reinforced concrete. Cement and Concrete Composites, 22(6), 407–415. doi:10.1016/S0958-9465(00)00040-8.

[64] Jaggi, S., Elsener, B., & Bohni, H. (2000). Oxygen Reduction on Mild Steel and Stainless Steel in Alkaline Solutions. Eurocorr 1999 Proceedings (London), 44–11.

[65] Hanaoka, D., Amino, T., Habuchi, T., Miyazato, S., & Tabata, S. (2015). A study on prediction method of chloride ion penetration into concrete with surface penetrants. Life-Cycle of Structural Systems: Design, Assessment, Maintenance and Management - Proceedings of the 4th International Symposium on Life-Cycle Civil Engineering, IALCCE 2014, 2014, 950–955. doi:10.1201/b17618-138.

[66] Zarzuela, R., Luna, M., Coneo, J. G., Gemelli, G., Andreouli, D., Kaloidas, V., & Mosquera, M. J. (2023). Multifunctional silane-based superhydrophobic/impregnation treatments for concrete producing CSH gel: Validation on mockup specimens from European heritage structures. Construction and Building Materials, 367, 130258. doi:10.1016/j.conbuildmat.2022.130258.

[67] Tanaka, H., Kurita, M., & Miyagawa, T. (2013). Prediction of chloride ion penetration for concrete impregnated with silane water-repellent material. Sustainable Construction Materials and Technologies, CRC Press, Florida, United States.

[68] Sakr, M. R., & Bassuoni, M. T. (2021). Silane and methyl-methacrylate based nanocomposites as coatings for concrete exposed to salt solutions and cyclic environments. Cement and Concrete Composites, 115, 103841. doi:10.1016/j.cemconcomp.2020.103841.

[69] Otieno, M., Ikotun, J., & Ballim, Y. (2019). Experimental investigations on the influence of cover depth and concrete quality on time to cover cracking due to carbonation-induced corrosion of steel in RC structures in an urban, inland environment. Construction and Building Materials, 198, 172–181. doi:10.1016/j.conbuildmat.2018.11.215.

[70] JSCE No. 17. (2007). Guidelines for Concrete No.17; Standard Specifications for Concrete Structures: Maintenance. Japan Society of Civil Engineers, Tokyo, Japan.

[71] Medeiros, M., & Helene, P. (2008). Efficacy of surface hydrophobic agents in reducing water and chloride ion penetration in concrete. Materials and Structures, 41, 59-71. doi:10.1617/s11527-006-9218-5.

[72] Kobayashi, S., Kurata, K., Hashimoto, M., Hayashi, D., Hasegawa, Y., Maeyama, A., and Endoh, H., (2023). 20-year exposure test results for silane-silaxone surface penetrant. Proceedings of 78th annual Academic lecture, National conference of the Japan Society of Civil Engineers, 2023 (Sep), East Hiroshima, V-316. (In Japanese).

[73] Zeng, Y., Zhang, D. wei, Dai, J. G., Fang, M. shan, & Jin, W. liang. (2020). Determining the service life extension of silane treated concrete structures: A probabilistic approach. Construction and Building Materials, 249, 118802. doi:10.1016/j.conbuildmat.2020.118802.

[74] Petcherdchoo, A. (2015). Environmental impacts of combined repairs on marine concrete structures. Journal of Advanced Concrete Technology, 13(3), 205–213. doi:10.3151/jact.13.205.

[75] Kuang, Y., Sakoi, Y., Takashima, N., Aba, M., & Tsukinaga, Y. (2022). Evaluation of the chloride ions penetration into concrete structure with the surface penetrants served in cold marine environment for 20 years. The 7th International Conference on Durability of Concrete Structures, ICDCS 2022, Shandong, China.

[76] Miyazato, S., & Takechi, S. (2016). Scenario designs from preemptive maintenance to preventive maintenance for aging concrete bridges with chloride attack". Proceedings of the EASEC-14 Special Session 3, The Fourteenth East Asia-Pacific Conference on Structural Engineering and Construction, 14, 319-328.

[77] Funakawa, I., Ushijima, S., Miyagawa, T., & Yamamoto, Y. (2005). Outline of Recommendation for Concrete Repair and Surface Protection of Concrete Structures by JSCE. Concrete Journal, 43(11), 3–11. doi:10.3151/coj1975.43.11_3.